Magnetic properties of stoichiometric Gd monopnictides

1997 J. Phys.: Condens. Matter 9 10777

(http://iopscience.iop.org/0953-8984/9/48/019)

J. Phys.: Condens. Matter **9** (1997) 10777–10788. Printed in the UK PII: S0953-8984(97)86241-8

Magnetic properties of stoichiometric Gd monopnictides

D X Li†‖, Y Haga†, H Shida†, T Suzuki†, Y S Kwon‡ and G Kido§

† Department of Physics, Tohoku University, Sendai, 980-77 Japan
‡ Department of Physics, Suny Kyun Kwan University, Suwon, South Korea
§ Tsukuba Magnet Laboratories, National Research Institute for Metals, Tsukuba, 305 Japan

Received 22 July 1997, in final form 3 October 1997

Abstract. We report on the systematic magnetization measurements performed on the stoichiometric Gd monopnictides, GdX_p (X_p = N, P, As, Sb, and Bi), at temperatures between 1.6 and 350 K in magnetic fields up to 42 T. GdN shows the ferromagnetic behaviour with a Curie temperature $T_c = 58$ K. The other GdX_p samples order antiferromagnetically at the Néel temperatures $T_N = 15.9$, 18.7, 23.4, and 25.8 K for X_p = P, As, Sb, and Bi, respectively. A spin–flop transition is observed at low temperature for GdX_p except GdN. Based on molecular field approximation, the nearest-neighbour and next-nearest-neighbour exchange constants J_1 and J_2 of GdX_p are calculated using the experimental data. Comparing with Eu monochalcogenides, the other group of S-state rare-earth compounds, the absolute values of J_1 and J_2 in GdX_p are anomalously large, and the ferromagnetic RKKY interactions due to semimetallic carriers are very weak. These anomalous properties are discussed with a new theoretical model developed very recently by Kasuya.

1. Introduction

Strongly correlated f-electron systems (SCES) have attracted much attention in the last decade due to their mysterious physical properties. The rare-earth monopnictides RX_p (X_p = N, P, As, Sb, and Bi) with NaCl-type structure are the most typical representatives of SCES with low carrier concentrations. Recently, success in preparing many high quality RX_p single crystals has made much progress experimentally. In particular, the Ce and Yb monopnictides, the electron-hole symmetry system, have been extensively investigated both experimentally and theoretically [1–3]. Various complicated physical phenomena, such as the dense Kondo effect, heavy-fermion states, magnetic ordering, crystalline-electric field (CEF) effect and the magnetic polaron effect etc have been observed in these compounds. Although some theoretical treatments have recently been developed by Kasuya *et al* [4–8] our understanding of the anomalous physical properties observed in RX_p is far from complete, because of the different effects that exist in different systems which compete with each other, making theoretical analysis difficult. Clearly, clarifying the mechanisms of the above-mentioned effects are the prerequisite of understanding the variety of physical properties in rare-earth monopnictides.

Indirect magnetic exchange interaction is considered to have the most important effect on the physical properties of RX_p compounds, and may vary in its characteristic from system to system. In order to understand the exchange mechanism more thoroughly, it is

‖ Present address: Oarai Branch, Institute for Materials Research, Tohoku University, Oarai, Ibaraki, 311-13 Japan. E-mail address: li@ob.imr.tohoku.ac.jp

0953-8984/97/4810777+12$19.50

desirable to have a 'model' material exhibiting only the exchange effect. This guides us to focus our attention on the Gd monopnictides. GdX_p is the most simple series in the RX_p family, because Gd is located in the centre of the series of the rare earths in the periodic table of the elements, the Gd^{3+} ion appearing in GdX_p has a $4f^7$ configuration and is an S-state ion with spin-$\frac{7}{2}$ and no orbital momentum. The CEF effects in GdX_p are considered to be fairly weak and the indirect exchange interactions are the main mechanism of the magnetic properties, while the anisotropic exchange and the multipole interactions are negligible. Therefore, GdX_p are the most suitable materials to study the magnetic exchange interactions in rare-earth compounds, and are the convenient reference systems for other rare-earth monopnictides. Similar to the other RX_p systems, GdX_p have the simple NaCl-type crystal structure, a weak overlap between the bottom of the conduction band and the top of the valence band make them semimetals with a low carrier concentration [9, 10]. Compared with La, Ce and Yb monopnictides, there have only been a few studies performed on powder GdX_p samples in the past. These have been carried out in a nonsystematic way for lack of high-quality samples. For GdN, there exist some controversies concerning its low-temperature magnetic structure, being classified as either a ferromagnet [11–14] or an antiferromagnet [15, 16]. The studies of magnetic properties and neutron diffraction on powder compounds of GdP, GdAs, GdSb, and GdBi suggest that they are type-II antiferromagnets below Néel temperatures T_N, and T_N depends strongly on the samples [12, 17, 18]. So far their intrinsic mechanisms of magnetic exchange interactions are still a puzzle. Systematic experiments on high-quality single crystals or stoichiometric samples are necessary.

However, to grow high-quality single crystals of GdX_p is very difficult due to the high weld point and high vapour pressure. Recently, we have succeeded in growing large stoichiometric and nonstoichiometric single crystals of GdP, GdAs, GdSb and GdBi, and in preparing stoichiometric polycrystal of GdN. The fundamental physical properties were measured carefully for all the samples. Some transport properties of the stoichiometric samples and the trapped magnetic polaron effects of the nonstoichiometric samples have been reported in our recent papers [19, 20]. In this paper, we present the magnetic properties of the stoichiometric polycrystal GdN and the single crystals GdP, GdAs, GdSb and GdBi. We shall show the high-field magnetization (M–H) and the low-field susceptibility (χ–T) behaviours, and determine some important magnetic parameters such as Néel temperature T_N (or Curie temperature T_C), paramagnetic Curie temperature θ_p, spin–flop transition field H_{sf} and the critical field (demagnetization field for GdN) H_c etc. Further, using these data the nearest-neighbour (NN) and next-nearest-neighbour (NNN) exchange constants J_1 and J_2 are calculated. We also show the anomalous characteristics of the magnetic exchange interactions in GdX_p and compare them with those in Eu monochalcogenides EuX_c (X_c = O, S, Se, and Te), another series of S-state 4f compounds. These anomalies are qualitatively discussed within the framework of Kasuya's model.

2. Experimental methods

The sample-preparation methods have previously been described in detail [20]. Single crystals of GdX_p are grown by the mineralization method (for X_p = P and As) and the Bridgman method (for X_p = Sb and Bi) in tungsten crucibles. For GdN, we applied a high-pressure method to prepare the powder sample for the first time by using a hot isostatic pressing furnace [21], that is, flakes of Gd metal in an open tungsten crucible are directly reacted with nitrogen at 1600 °C and a N_2 pressure of 1300 atm for 3 h. X-ray diffraction patterns show a single phase of NaCl-type for all the GdX_p samples. The room-temperature

Table 1. Lattice constants a, Néel temperatures T_N (Curie temperature T_c for GdN), paramagnetic Curie temperatures θ_p, spin–flop transition fields H_{sf}, critical fields (demagnetization field for GdN) H_c, saturation fields H_s, NN exchange constants J_1, and NNN exchange constants J_2 are listed for Gd monopnictides.

	GdN	GdP	GdAs	GdSb	GdBi
a (Å)	4.974	5.709	5.864	6.219	6.295
T_N (K)	58.0 (T_c)	15.9	18.7	23.4	25.8
θ_p (K)	81.0	4.0	−11.8	−31.3	−45.0
H_{sf} (T)		0.3	0.2	0.2	0.5
H_c (T)	0.8	9.6	16.7	34.5	∼42.0
H_s (T)	1.5	11.0	18.0	35.0	∼43.0
J_1 (K)	0.64	0.22	0.08	0.05	−0.04
J_2 (K)	0	−0.34	−0.35	−0.60	−0.63

lattice constants are listed in table 1. Except for the polycrystalline GdN sample, the electric resistivity, magnetoresistivity and de Haas–van Alphen (dHvA) effect measurements show the GdX_p samples to be high-quality single crystals [20]. The atomic ratios between Gd and pnictogen determined by chemical analysis are $1{:}1.00 \pm 0.01$ for the five stoichiometric samples.

The measurements of the temperature dependence of magnetization are carried out in the temperature range of about 1.7–350 K using a superconducting quantum interference device (SQUID) magnetometer. The high-field magnetizations are measured by using a pulse magnetic field ($0 \leqslant H \leqslant 42$ T), while the low-field magnetizations ($H \leqslant 1$ T) are measured in detail with the quantum design SQUID magnetometer that was used for the susceptibility measurements.

3. Experimental results

3.1. Ferromagnetic polycrystal GdN

Figure 1 shows the temperature dependence of the reduced magnetization M/H of GdN at different magnetic fields. In order to reduce the observational error, the measurements for $H = 0.0002$ and 0.0005 T were carried out using a sample about ten times larger than that used for the high-field measurements. Wachter *et al* [15] found a sharp peak at 40 K in their susceptibility measurements in a field of 0.001 T for GdN, and claimed that this sharp peak represents an antiferromagnetic transition. Our experiments for the GdN sample, however, do not give any evidence for antiferromagnetism even at $H = 0.0002$ T. Indeed, in many less perfect samples nonferromagnetic-type orderings are observed [15, 22]. Therefore, it seems that in pure GdN the ferromagnetic ordering appears. In this respect, the stoichiometry in our GdN sample seems better. For $T > 230$ K, $(M/H)^{-1}$ curves show Curie–Weiss behaviour. From the data for $230 < T < 350$ K, we determined the paramagnetic Curie temperature $\theta_p = 81$ K and effective magnetic moment $\mu_{eff} = 7.92\mu_B$ at $H = 0.05$ T.

The magnetization data of GdN are plotted in the inset of figure 1. The measurements at 1.6 and 4.2 K reveal only small difference in the field dependence of the Gd^{3+} magnetic moments with saturation values being reached at about 1.5 T. The saturation moments of $6.84\mu_B/Gd^{3+}$ and $6.88\mu_B/Gd^{3+}$ at 4.2 and 1.6 K, respectively, are approximately 2% below the theoretical value of $7.0\mu_B$ per Gd^{3+}. A similar behaviour has been reported by

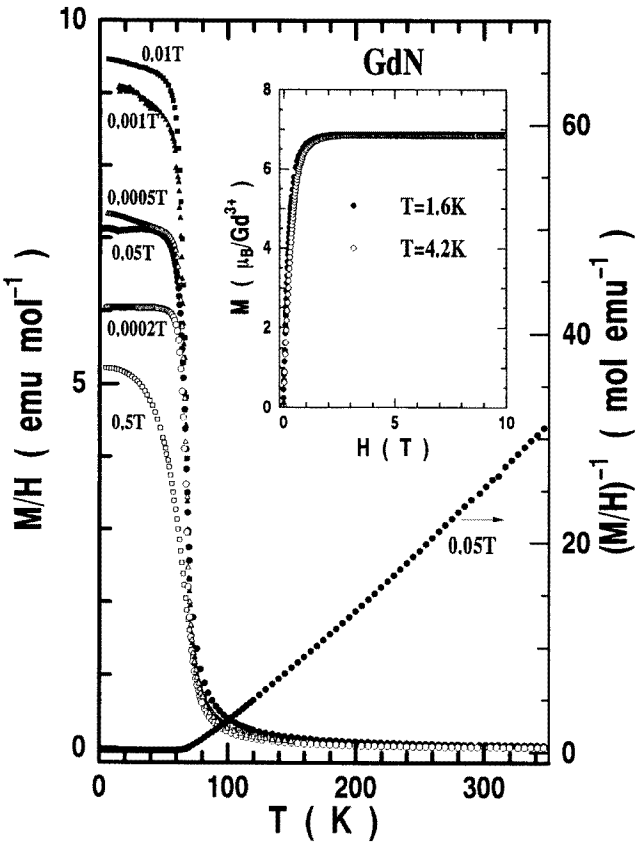

Figure 1. Temperature dependencies of the reduced magnetization (M/H) and the inverse reduced magnetization (H/M) of GdN in different magnetic fields. The inset shows the magnetization of GdN measured at $T = 1.6$, and 4.2 K and $H \leqslant 10$ T.

Gambino *et al* [13]. At low fields, the magnetic moment of GdN increases rapidly and is nonlinear as in a ferromagnet, however, it did not show evident hysteresis effects for measurements carried out in increasing and decreasing magnetic fields. The results shown in figure 1 correspond to ferromagnetic behaviour despite the absence of a clear hysteresis effect. The Curie temperature T_c was determined to be 58 K from figure 1, which agrees with our specific heat measurements very well [21].

Note that the experimental M/H value at the lowest temperature shows a strong field dependence, and does not steadily decrease as a function of the applied field. This behaviour can be observed in some ferromagnets due to the fact that the magnetization curve (M–H) is nonlinear, i.e. it bends upward at very low fields and downward at relatively high fields. The physical reason might be rather complex relating to the demagnetization effects, internal stresses and lattice defects etc. Thus we cannot at present clearly explain this phenomenon observed in GdN. Nevertheless the demagnetization effect in GdN seems to be weak, because the hysteresis effect is not evident, and the above-mentioned phenomenon was observed for measurements (M/H–T curves) carried out with increasing applied field.

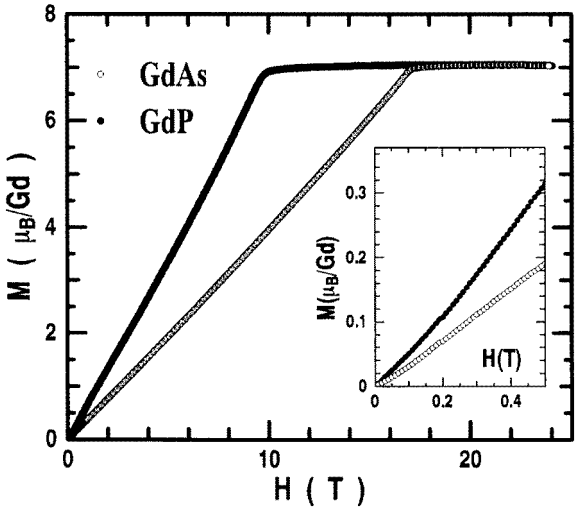

Figure 2. Magnetic field dependencies of the magnetizations of GdP and GdAs at $T = 4.2$ K and in the $H \parallel [100]$ direction. The inset shows the low-field parts.

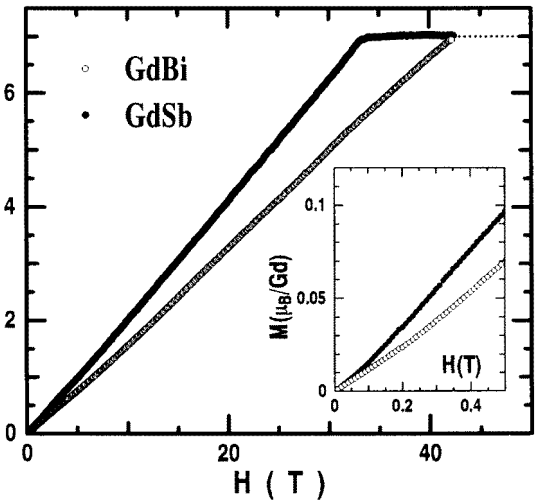

Figure 3. Magnetic field dependence of the magnetization of GdSb and GdBi at $T = 4.2$ K and in the $H \parallel [100]$ direction. The inset shows the low-field parts.

3.2. Antiferromagnetic single crystals GdP, GdAs, GdSb and GdBi

The field dependences of the magnetization are displayed in figure 2 for GdP and GdAs, and in figure 3 for GdSb and GdBi. The measurements were carried out at $T = 4.2$ K and in the $H \parallel [100]$ direction. For GdP, GdAs, and GdSb, the saturation moment is about $7.01\mu_B/Gd^{3+}$. For GdBi, although the magnetization is not saturated up to 42 T, the moment at 42 T has reached the theoretical saturation value, $7.0\mu_B/Gd^{3+}$. The low-field parts of the magnetization curves of GdX_p are nonlinear as shown in the insets of figures 2 and 3. Extrapolations of the H-linear part of the magnetization curves intercept with the H-axis at 0.04, 0.02, 0.02 and 0.05 T for GdP, GdAs, GdSb and GdBi, respectively. This

suggests that a spin–flop transition occurs at low field and the anisotropy field is very small as expected for S-state systems.

In order to analyse the above experimental results, the dM/dH curves are illustrated in figure 4 for GdP and GdAs and in figure 5 for GdSb and GdBi. It is clear from these figures that two peaks are observed at both a lower field H_{sf} and a higher field H_c. These represent phase transitions from the antiferromagnetic phase to the spin–flop phase and from the spin–flop phase to the paramagnetic phase (with induced saturation moment), respectively. The spin–flop transition in GdX_p can be understood as follows. Neutron diffraction experiments revealed that GdX_p, except GdN, are the cubic antiferromagnets with magnetic order of type II [12, 17, 18], thus the four equivalent {111} planes are the easy planes for the sublattice magnetizations. At zero field and below T_N, M_1 and M_2, the sublattice magnetizations, are antiparallel with each other and point along certain directions. When a magnetic field H is applied, at certain values of H ($= H_{sf}$), M_1 and M_2 should rotate abruptly in the {111} planes toward the directions which are nearly perpendicular to H. This process is analogous to the spin–flop transition in uniaxial antiferromagnet. At H_{sf} the curve of dM/dH has a sharp peak. From figures 4 and 5, the spin–flop transition fields H_{sf} in our GdX_p samples are evaluated to be about 0.3, 0.2, 0.2, and 0.5 T for $X_p =$ P, As, Sb and Bi, respectively. Note that the transition peaks around H_{sf} in GdX_p are not so sharp, the reason may be that the direction of H (applied along [100]) deviates from $\pm n$, the unit vectors of M_1 and M_2, so that the transition should take place gradually as described in [23] for EuTe.

It is also clear from figures 4 and 5 that dM/dH exhibits a λ peak at high field for GdP, GdAs and GdSb. We choose to identify the field where dM/dH is maximum with H_c. Above H_c, dM/dH decreases abruptly with H, and drops to near zero at $H = H_s$. In the spin–flop phase the sublattice magnetizations M_1 and M_2 are canted relative to each other by an angle. As H increases the canting angle increases until M_1 and M_2 become parallel relative to each other and to H at $H = H_c$, while a second-order phase transition from spin–flop phase to paramagnetic phase happens. This transition is characteristic of a λ peak in the dM/dH curve. Thus H_c in figures 4 and 5 is defined as the critical magnetic field, while H_s is the saturation field. The former represents the start of the transition and the latter the end of the transition. From figures 4 and 5, H_c and H_s are evaluated to be 9.6 and 11.0 T for GdP, 16.7 and 18.0 T for GdAs, and 34.5 and 35.0 T for GdSb, as listed in table 1. For GdBi, because the magnetization value has reached the theoretical saturation value, $7.0\mu_B/Gd^{3+}$, at $H = 42$ T, H_c and H_s are estimated to be about 42 and 43 T, respectively.

The reduced magnetization $\chi = M/H$ (also called susceptibility at very low fields) was measured as a function of T at $H = 0.01$ T ($H \parallel [100]$) for GdP, GdAs, GdSb, and GdBi. The results are shown in figure 6. The four samples show similar behaviours which can be described as follows. (1) χ is Curie–Weiss-like at higher temperatures, as can be seen from the χ^{-1} curve. Using the expression $\chi = C/(T - \theta_p)$, here $C = N_A\mu_{eff}^2/(3k_B)$, the best fits of the data above 100 K yield $\theta_p = 4.0$, -11.8, -31.3, and -45.0 K and $\mu_{eff} = 8.18$, 8.15, 7.91, and $8.20\mu_B$ for GdP, GdAs, GdSb, and GdBi, respectively. (2) At low temperatures, a sharp peak characteristic of the antiferromagnetic transition is observed for all the samples. The Néel temperature is identified as the temperature of the peak in the $d(T\chi)/dT$ curve, which gives $T_N = 15.9$ K for GdP, 18.7 K for GdAs, 23.4 K for GdSb and 25.8 K for GdBi. With increasing H, T_N of GdX_p evidently does not change up to 0.5 T. (3) For GdAs, χ reduces to 0.162 emu mol^{-1} at 5 K, this value is close to $\frac{2}{3}\chi_{max}$, where $\chi_{max} = 0.225$ emu mol^{-1} is the maximum value of χ reached just above T_N. Similar features are also observed in GdP, GdSb and GdBi. Note that the relation of $\chi(T \to 0) = \frac{2}{3}\chi_{max}$ refers to Heisenberg antiferromagnetic polycrystals and our measurements refer to the single crystals. This again indicates that the magnetic anisotropy is very weak in S-state GdX_p.

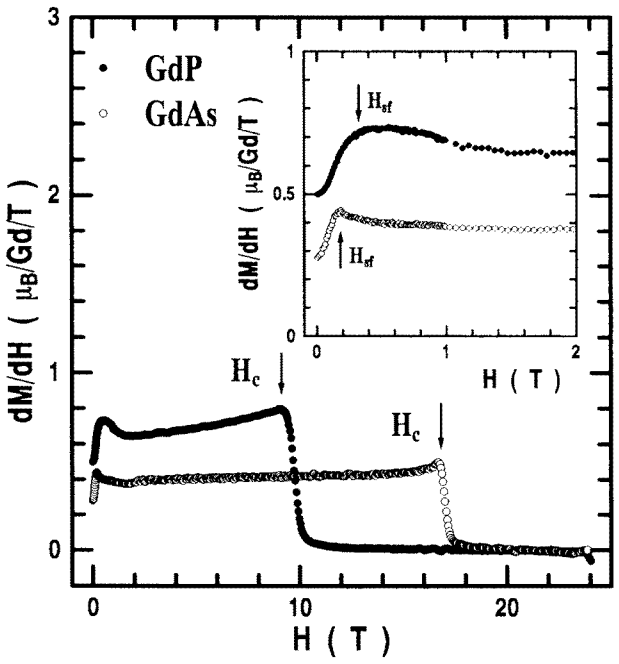

Figure 4. Differential magnetization dM/dH versus applied magnetic field for GdP and GdAs at 4.2 K. The inset shows the details below 1 T.

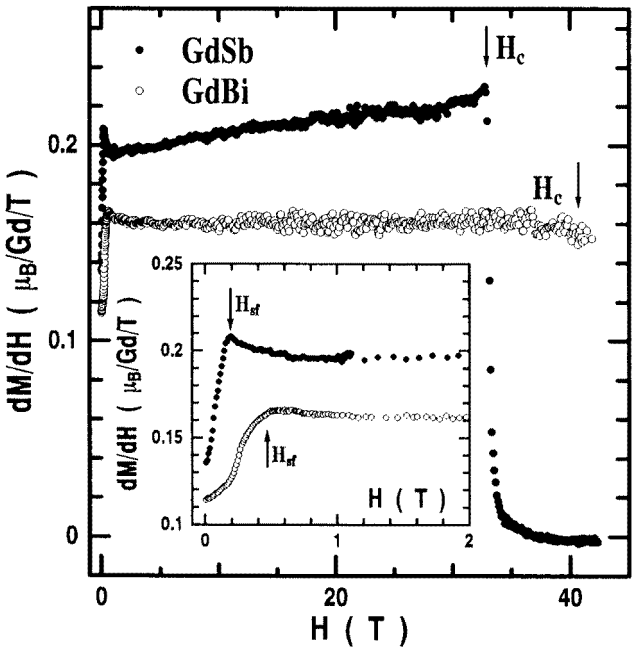

Figure 5. Differential magnetization dM/dH versus applied magnetic field for GdSb and GdBi at 4.2 K. The inset shows the details below 1 T.

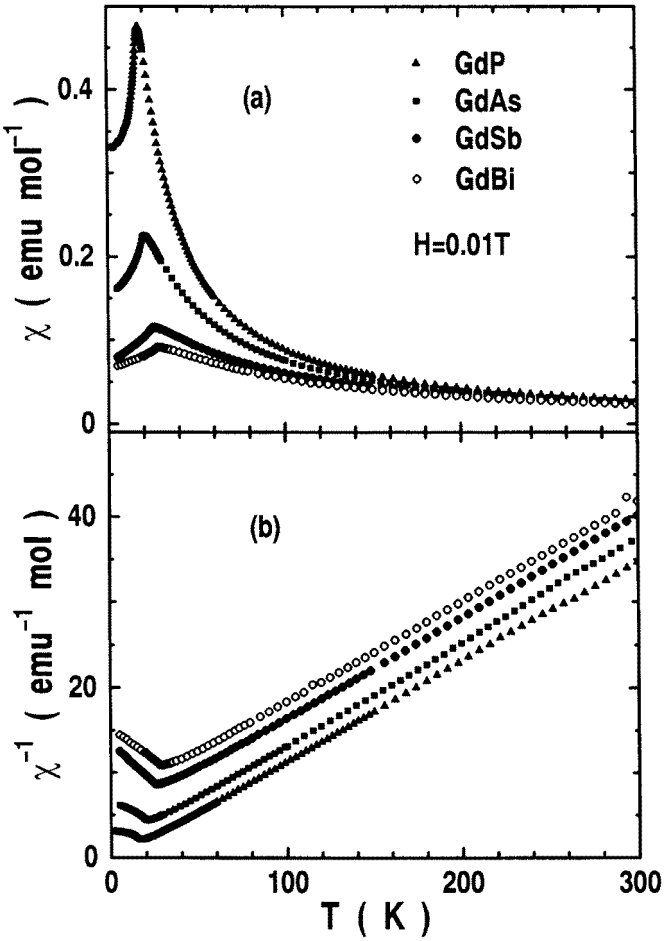

Figure 6. Temperature dependencies of (*a*) the reduced magnetization $\chi = M/H$ and (*b*) the inverse reduced magnetization $\chi^{-1} = H/M$ of GdP, GdAs, GdSb, and GdBi in a magnetic fields of 0.01 T with $H \parallel [100]$ direction.

4. Discussion

There are many puzzles on the mechanisms of exchange interactions in Gd monopnictides, in particular in ferromagnetic GdN. Phenomenologically, GdX_p seem to behave like the general ferromagnetic or antiferromagnetic Eu monochalcogenides. Careful analysis, however, indicates that essential distinctions exist in the exchange mechanisms between these two groups. In the following, we will first calculate the NN and NNN exchange constants J_1 and J_2 using the molecular field approximation, then compare the results with those of EuX_c, and finally discuss the difference of exchange mechanisms between GdX_p and EuX_c.

The exchange interaction between Gd ions in GdX_p can be described in terms of an interaction of each Gd^{3+} ion with its 12 NNs and six NNNs. Excepting GdN, all other GdX_p exhibit long-range fcc antiferromagnetic type-II ordering, thus the experimental values of T_N, θ_p, and $H_c(0)$ can be used to evaluate the NN and NNN exchange constants J_1 and J_2

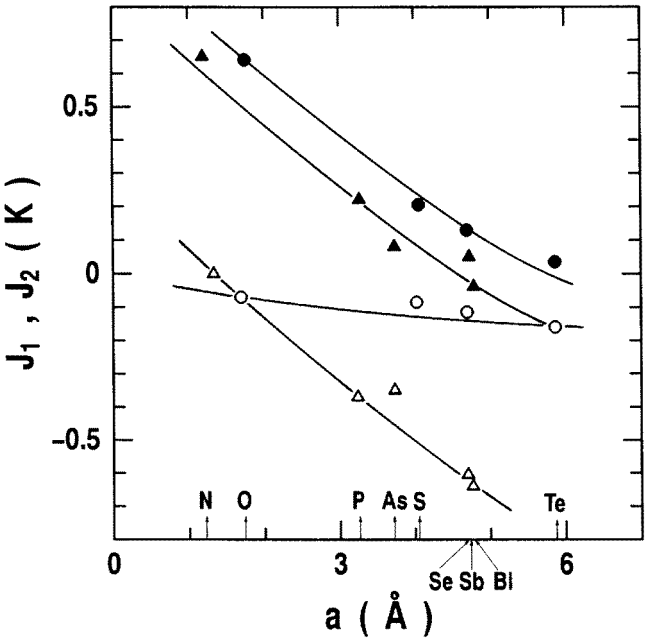

Figure 7. NN and NNN exchange constants J_1 and J_2 for Gd monopnictides (▲ and △, respectively) and Eu monochalcogenides (● and ○, respectively) are plotted as functions of lattice constant a.

by using the molecular field approximation. The equations relating T_N, θ_p, and $H_c(0)$ are

$$k_B T_N = -63 J_2 \tag{1}$$

$$k_B \theta_p = 126 J_1 + 63 J_2 \tag{2}$$

$$g\mu_B H_c(0) = -84(J_1 + J_2). \tag{3}$$

Note that T_N is strongly affected by short-range ordering and thus equation (1) will underestimate J_2. Therefore, H_c is more generally valid than T_N for estimating J_1 and J_2. We used equations (2) and (3) to calculate J_1 and J_2, the results are shown in table 1. For all four single-crystal samples, the antiferromagnetic NNN interaction J_2 is stronger than the ferromagnetic NN interaction J_1, this is a general feature for a Heisenberg antiferromagnet. For GdN, because it shows ferromagnetic behaviour, J_1 was evaluated from θ_p simply by assuming $J_2 = 0$. In figure 7 the J_1 and J_2 of GdX_p are plotted against the lattice constant a and compared with those of EuX_c [24]. The value of J_1 in both GdX_p and EuX_c decreases rapidly with increasing a. The antiferromagnetic interaction J_2 depends on a strongly for GdX_p, and weakly for EuX_c.

It is well known that both GdX_p and EuX_c crystallize in the NaCl-type structure with essentially the same band structure. Both Gd^{3+} and Eu^{2+} have the $4f^7$ configuration with $S = \frac{7}{2}$ and $L = 0$. The bottom of the conduction bands is at each X-point of the Brillouin zone formed mainly by the t_{2g} type of 5d(R), R represents Gd or Eu. The top of the valence band formed mainly by $p(X_p$ or $X_c)$ is at the Γ-point, and splits into Γ_8 quartet and Γ_6 doublet by the spin–orbit interaction [9]. In EuX_c, band gaps between the conduction and valence bands are about 2–4 eV making them insulators. The occupied 4f levels lie in the gap, about 2–4 eV apart from the Fermi energy E_F, and the unoccupied 4f levels lie about 12–14 eV above E_F [25]. In GdX_p, however, a weak overlap between the bottom of

the conduction band and the top of the valence band makes them semimetals with carrier numbers of a few per cent per Gd. The occupied and unoccupied 4f levels in GdX_p are situated 8–10 and 5–6 eV below and above Fermi energy E_F, respectively [26, 27].

EuX_c are the first rare-earth compounds studied extensively on high-quality samples because of their interesting novel properties. The mechanism of the strong ferromagnetic NN exchange constant J_1 in EuO and its strong lattice constant a dependence in going from EuO to EuTe were explained by Kasuya *et al* [28, 29] as follows. Through f–d mixing, an occupied 4f electron can be transferred to the 5dt_{2g} excited state of a NN Eu site, where the 5d electron polarizes the occupied 4f spins ferromagnetically parallel to the 4f spins at the centre Eu site through strong intra-atomic d–f exchange interaction. the strong a dependence of J_1 shown in figure 7 is due to strong a dependence of the d–f mixing. On the other hand, the NNN exchange constant J_2 is considered to originate from the conventional superexchange mechanism through the fourth order of p–f mixing and thus J_2 depends weakly on a.

GdX_p are similar in their fundamental characteristics, band structures and lattice constants with the corresponding EuX_c. Gd^{3+} has the same $4f^7$ configuration as Eu^{2+}. Thus the same d–f and p–f mixing mechanisms existing in EuX_c are naturally considered to exist also in GdX_p. In third-order perturbation of the energy, J_1 is proportional to U_{fd}^{-2}, the separation of the 4f and the 5dt_{2g} levels. Because U_{fd}^{-2} is 2–3 eV in EuX_c and 8–10 eV in GdX_p, J_1 is expected to be at least 10 times smaller in GdN than in EuO. However, the results evaluated from θ_P and H_c by using the molecular-field approximation show that as a function of a, J_1 in GdX_p and EuX_c are nearly on a universal curve, even though the values for GdX_p are slightly below those for EuX_c (figure 7). This leads to the consideration that the additional RKKY indirect-exchange interaction, due to the semimetallic carriers, seems to be present in these systems [12, 15]. Thus the large positive J_1 in GdN and large negative J_2 in GdSb and GdBi are naturally explained as follows [15]. The carrier concentration n in GdX_p increases in going from GdN to GdBi, which may affect the value and sign of θ_p, because the RKKY interaction is oscillatory with increasing carrier concentration. n in GdN lies the range which makes the RKKY oscillation in the ferromagnetic lobe, while n in other GdX_p lies the range which makes the RKKY oscillation in the antiferromagnetic lobe. However, the band calculation [9], Hall-effect and dHvA-effect measurements [20] have shown that n in GdX_p is too small for antiferromagnetic RKKY interaction, only a few percent per Gd even in GdBi. Thus we rather expect a ferromagnetic RKKY interaction in all the Gd monopnictides [15].

To solve this puzzle and understand the mechanisms of magnetic exchange interactions in the Gd monopnictides, a new theoretical model has very recently been developed by Kasuya, and has been described in recent letters [30, 31]. The basic idea is the following. The large positive J_1 in GdN can be explained by the cross process between the d–f mixing and d–f exchange interaction to form the $4f^8$ configuration, in which the added 4f electron should have the opposite spin direction to that of the $4f^7$ configuration. The lowest-order process is of the fourth order, for example the $p(N) \rightarrow 4f^8 \rightarrow 5d(NNGd) \rightarrow$ d–f exchange $\rightarrow p(N)$ and its reverse process, giving the following coupling constant:

$$J_1' = -4I_{df}t_{pf}t_{fd}t_{dp}/SU_{pf}U_{pd}^2 \tag{4}$$

where I_{df} is the intra-atomic d–f exchange interaction constant, U_{pf} and U_{pd} are the separations between the 4f level and the p band, and between the 4f level and the 5d band. $2t_{pf}t_{fd}t_{dp}$ means the summation over the seven unoccupied 4f states. Because the $p(N)$ state sits in between the two NN Gd atoms under consideration, the sign of $t_{pf}t_{fd}t_{dp}$ is negative and thus J_1' is positive, i.e. ferromagnetic. J_1' is evaluated to be small in EuO,

because the value of U_{pd} is large, making J_1' in EuO negligible compared with J_1. In GdN, however, J_1' is evaluated to be about 0.5–1J_1 in EuO and thus, the total J_1 in GdN is nearly equal to J_1 in EuO [30]. The above mechanism is also weak in other GdX_p, because of the strong distance dependence of the d–f mixing interaction.

The antiferromagnetic NNN exchange constant J_2 in GdX_p is considered to originate from the superexchange mechanism through the fourth-order process of p–f mixing, similar to that in EuX_c. This is consistent with the larger J_2 values in GdX_p because of their smaller value of U_{pf}.

It is well known that when carriers of a few per cent per Eu atom are induced by substituting trivalent R (R = rare-earth elements) for Eu in EuX_c, the paramagnetic Curie temperature θ_p increases up to 30–40 K [22, 32] due to the ferromagnetic RKKY interaction, and the systems change from antiferromagnetism to ferromagnetism. In GdX_p, the carrier concentration is also a few per cent per Gd, and thus the situation is similar to that of R^{3+} doped EuX_c. However, no marked increase in θ_p is observed in GdX_p, and thus large negative J_2 is observed. This means that the RKKY interaction resulting from the free carriers is weak in GdX_p, further, the band states near E_F in GdX_p must be different from those in EuX_c, because these band states are responsible for θ_p. This anomalous property can be explained as the cancellation of the ferromagnetic d–f exchange interaction and the antiferromagnetic p–f scattering through the second-order process of p–f mixing with opposite signs [33]. Independent evidence to confirm this cancellation effect is the small spin-disorder magnetic resistivity in GdX_p, in particular in GdSb and GdBi [20]. This kind of cancellation effect is important only in low carrier density systems with small scattering wavevectors, and the semimetallic GdX_p is the first case to show the cancellation clearly.

In conclusion, systematic magnetic measurements on the high-quality stoichiometric GdX_p (X_p = N, P, As, Sb and Bi) samples showed that the polycrystal GdN is a ferromagnet with a Curie temperature $T_c = 58$ K. Single crystals GdP, GdAs, GdSb and GdBi behave like the antiferromagnets with the Néel temperatures $T_N = 15.9$, 18.7, 23.4, and 25.8 K, respectively, while the spin–flop transitions are also observed at low magnetic fields for them. Based on the molecular-field approximation, the NN and NNN exchange constants J_1 and J_2 are calculated for the Gd monopnictides using the Néel temperatures T_N (Curie temperature T_c for GdN), paramagnetic Curie temperatures θ_p, critical fields (demagnetization field for GdN) H_c and saturation fields H_s determined in this study. Even though the relative energy levels are substantially different in Gd monopnictides and Eu chalcogenides, the calculated results for the two series reveal only small differences in the lattice constant dependence of the NN exchange constant J_1. On the other hand, in contrast to the R^{3+} doped EuX_c, although the carriers of several per cent per Gd exist in GdX_p, the ferromagnetic RKKY interaction is very weak for them. This anomalous behaviour can be qualitatively understood within the framework of Kasuya's model. The former is attributed to the cross processes between the f–d mixing and the f–d exchange interaction, and the latter is explained as the cancellation of the intra- and inter-site d–f scattering characteristic to GdX_p.

Acknowledgment

DXL wishes to thank Professor T Kasuya for helpful advice.

References

[1] Suzuki T 1993 *Japan. J. Appl. Phys.* **8** 267

[2] Suzuki T 1993 *J. Phys. B: At. Mol. Opt. Phys.* **186&188** 347
[3] Kasuya T, Suzuki T and Haga Y 1993 *J. Phys. Soc. Japan* **62** 2549
[4] Kasuya T 1993 *J. Alloys Compounds* **192** 217
[5] Kasuya T, Haga Y, Kwon Y S and Suzuki T 1993 *J. Phys. B: At. Mol. Opt. Phys.* **186–188** 9
[6] Kasuya T, Haga Y, Suzuki T, Kaneta Y and Sakai O 1992 *J. Phys. Soc. Japan* **61** 3447
[7] Kasuya T, Oyamada A, Sera M, Haga Y and Suzuki T 1994 *J. Phys. B: At. Mol. Opt. Phys.* **199–200** 585
[8] Kasuya T and Li D X 1997 *J. Phys. Soc. Japan* **66** 1587
[9] Hasegawa A and Yanase A 1977 *J. Phys. Soc. Japan* **42** 492
[10] Kasuya T, Sakai O, Tanaka J, Kitazawa H and Suzuki T 1987 *J. Magn. Magn. Mater.* **63&64** 9
[11] Busch G 1967 *J. Appl. Phys.* **38** 1386
[12] McGuyre T R, Gambino R J, Pickart S J and Alperin H A 1969 *J. Appl. Phys.* **40** 1009
[13] Gambino R J, McGuyre T R, Alperin H A, Pickart S J and Alperin A 1970 *J. Appl. Phys.* **41** 933
[14] Stutius W 1969 *Phys. Kondens. Mater.* **10** 152
[15] Wachter P and Kaldis E 1980 *Solid State Commun.* **34** 241
[16] Cutler R A and Lawson A W 1975 *J. Appl. Phys.* **46** 2739
[17] Nereson N and Struebing V 1972 Magnetism and magnetic materials *Proc. 17th Annual Conf. on Magnetism and Magnetic Materials (Chicago, IL, 1971) (AIP Conf. Proc. 5)* ed C D Graham Jr and J J Phyne (New York: AIP) p 1385
[18] Hulliger F 1979 *Handbook on the Physics and Chemistry of Rare Earths* vol 4, ed K A Gschneidner Jr and L R Eyring (Amsterdam: North-Holland) p 191
[19] Li D X, Haga Y, Shida H, Suzuki T, Koide T and Kido G 1996 *Phys. Rev.* B **53** 8473
[20] Li D X, Haga Y, Shida H, Suzuki T and Kwon Y S 1996 *Phys. Rev.* B **54** 10 483
[21] Li D X, Haga Y, Shida H and Suzuki T 1994 *Physica* B **199&200** 631
[22] Narita A and Kasuya T 1985 *J. Magn. Magn. Mater.* **52** 373
[23] Oliveira N F Jr, Foner S, Shapira Y and Reed T B 1972 *Phys. Rev.* B **5** 2634
[24] Fukuma H 1985 *PhD Thesis* Tohoku University
[25] Cho S 1967 *Phys. Rev.* **157** 632
[26] Kasuya T 1970 *J. Appl. Phys.* **41** 1090
[27] Yamada H, Fukawa T, Muro T, Tanaka Y, Imada S, Suga S, Li D X and Suzuki T 1996 *J. Phys. Soc. Japan* **65** 1000
[28] Kasuya T 1972 *Crit. Rev. Solid State Sci.* **3** 131
[29] Sakai O, Yanase A and Kasuya T 1977 *J. Phys. Soc. Japan* **42** 596
[30] Kasuya T and Li D X 1997 *J. Magn. Magn. Mater.* **167** L1
[31] Kasuya T and Li D X 1997 *Physica* B **230–232** 472
[32] Holtzberg F, McGuire T R, Methfessel S and Suits J C 1964 *Phys. Rev. Lett.* **3** 18
[33] Kasuya T and Li D X 1997 *J. Magn. Magn. Mater.* **166** L1